Exploring Observation-Domain with Nonlinear Time-Series Warping for Aided GNSS Navigation

Francesco Fiorina, Oliviero Vouch, Andrea Nardin, Fabio Dovis
Dept. of Electronics & Telecommunications (DET)
Politecnico di Torino
Turin, Italy
name.surname@polito.it

***Abstract*—This paper investigates the application of sequence matching (SM) techniques to enhance aided GNSS navigation in lunar mission scenarios. Focusing on the challenges of aligning GNSS-derived Position, Velocity, and Time (PVT) solutions with pre-designed Aiding Trajectories (ATs) under varying geometric conditions, the study identifies Dynamic Time Warping (DTW) as the most effective SM strategy. The novelty lies in extending nonlinear time-series warping methods towards the exploration of the observation domain, introduced as a promising alternative of our previous work based on a state domain approach. Merging GNSS observations as primary data sequences avoids the burden of GNSS-only state estimation—particularly limited in cislunar environments—while enabling data fusion at an earlier stage of processing. A key advantage of the observation domain is its ability to support multidimensional sequence matching even in low-visibility conditions typical of high-altitude navigation. Throughout this work, our aim is to refine weighting strategies and expand the use of observation-domain SM for deep-space navigation and signal processing, leveraging the flexibility and robustness it offers to address geometric challenges in lunar GNSS applications.**

***Index Terms*—Global Navigation Satellite System, Dynamic Programming, Space communications, Space exploration, Lunar Mission, Dynamic Time Warping**

I. Introduction

The space sector is rapidly expanding, entering a new era of deep-space exploration. As missions scale up, the demand for accurate and autonomous Orbit Determination (OD) and Position, Velocity, and Time (PVT) estimation is increasing.

Currently, spacecraft navigation, positioning and maneuvering rely on ground-based assets such as National Aeronautics and Space Administration (NASA)'s Deep Space Network (DSN) [1], [2] and European Space Agency (ESA)'s European Space Tracking Network (ESTRACK), which provide tracking and communication support. Moreover, on-board measurements like Doppler measurements and two-way ranging are used in combination with these assets. These methods, while effective, have limitations, including high operational costs, resource constraints, complex infrastructure, and latency issues [3], [4]. To address these challenges, Global Navigation Satellite System (GNSS) is being explored as a potential alternative.

A notable example is the Lunar GNSS Receiver Experiment (LuGRE), a joint NASA-Agenzia Spaziale Italiana (ASI) payload on the Firefly Blue Ghost Mission 1 (BGM1) mission, designed to demonstrate GNSS capabilities beyond 30 Earth Radii (RE). In particular Position, Navigation, and Timing (PNT) will be demonstrated at Moon surface and during the Moon Transfer Orbit (MTO) [5]–[7].

Various methods have been proposed to improve OD using GNSS, including the Orbital Filter (OF) in [8], which leverages an Extended Kalman Filter (EKF) framework. However, at higher altitudes, these approaches face accuracy issues due to weak signals and high Geometric Dilution Of Precision (GDOP). To address these limitations, an advanced OF was developed in [9], while authors in [4] proposed the Trajectory-Aware Extended Kalman Filter (TA-EKF), which optimally fuses GNSS data with pre-mission trajectory information (*Aiding Trajectory (AT)*). However, the lack of time alignment between these data sources and the potentially different sample rates introduce additional challenges [3], [4]. The solution to this issue is investigated in a previous work [10], where Sequence matching (SM) techniques are applied to align two sequences. Specifically, SM is performed between sequences of states, including the spacecraft positions and velocities. This work introduces a novel post-processing application of the same SM technique to a different type of sequence. Specifically, it applies the method to observables (i.e. pseudoranges and pseudorange rates) instead of states. Compared to previous approaches, this represents a tighter SM, as it operates directly on raw measurement data. An effective SM is thus crucial to a subsequent integration of aiding information into estimation algorithms like the TA-EKF. This work uses preparatory data from the LuGRE project as a case study.

II. The Sequence Matching problem and its solution

SM involves finding meaningful matches between elements (also called *samples*) of two sequences. These sequences represent the evolution over time of a point in a multidimensional space. In this context, they can be modeled as Variable-Dimension Multi Dimensional Sequences (VDMDSs), consisting of a time-ordered sequence of Multi-Dimensional Sequences (MDSs). Each MDS is a matrix which dimensions may change from the other MDSs associated to different time instants. In the context of this work, the two VDMDSs for which we seek alignment are

- a *GNSS observables-based trajectory* $\mathbf{P} = \{\mathbf{P}_1, \ldots, \mathbf{P}_k, \ldots, \mathbf{P}_K\}$, which is a VDMDS having $\mathbf{P}_k = [\mathbf{P}_k^{\rho}, \mathbf{P}_k^{\dot{\rho}}]$ as a entry, which is a MDS. Each $\mathbf{P}_k$ is composed by $\mathbf{P}_k^{\rho} \in \mathbb{R}^{1,L_k}$ and $\mathbf{P}_k^{\dot{\rho}} \in \mathbb{R}^{1,L_k}$ where $\mathbf{P}_k^{\rho}$ contains L_k pseudorange measurements and $\mathbf{P}_k^{\dot{\rho}}$ contains L_k pseudorange rates, both measured at epoch k. The number L_k of Satellite Vehicles (SVs) in Line of Sight (LOS) can vary at each epoch. Each entry $\mathbf{P}_k \in \mathbb{R}^{1,2L_k}$ has the following form similar to the red equation representing $\mathbf{P}_1$ in Fig. 1.
- an *Observables-Based Aiding Trajectory (OBAT)* $\mathbf{P}_{\text{AID}} = \{\mathbf{P}_{\text{AID},1}, \ldots, \mathbf{P}_{\text{AID},k}, \ldots, \mathbf{P}_{\text{AID},K}\}$ is a VDMDS containing the aiding measurements, consisting in synthetic pseudoranges and pseudorange rates. Each entry $\mathbf{P}_{\text{AID},k} = [\mathbf{P}_{\text{AID},k}^{\rho}, \mathbf{P}_{\text{AID},k}^{\dot{\rho}}]$ is a MDS, where: $\mathbf{P}_{\text{AID},k}^{\rho} \in \mathbb{R}^{N,L_k}$ and $\mathbf{P}_{\text{AID},k}^{\dot{\rho}} \in \mathbb{R}^{N,L_k}$. $\mathbf{P}_{\text{AID},k}^{\rho}$ contains N synthetic pseudorange measurements for each l_k-th SV, and $\mathbf{P}_{\text{AID},k}^{\dot{\rho}}$ contains N synthetic pseudorange rate measurements for each l_k-th SV. The number of SVs in LOS can vary over time; for this reason, a new set of N aiding pseudoranges and pseudorange rates for each visible SV l_k is considered at each epoch k. An example of the final aiding measurements matrix is reported in red in Fig. 1 for $\mathbf{P}_{\text{AID},1}$.

A. Problem statement

To guarantee that a single sample of $\mathbf{P}$ is uniquely matched with only one sample of $\mathbf{P}_{\text{AID}}$ it is necessary to solve an optimization problem. The final result must be a time-consistent match, meaning that the samples from the two VDMDS are aligned in time. This requirement is enforced by introducing specific constraints into the problem formulation. The problem satisfying these conditions is formalized in [10] and is adapted here to address the case under study:

$$\mathbf{S}^* = \arg\min_{\mathbf{S}} \; f(\mathbf{P}, \mathbf{P}_{\text{AID}}, \mathbf{S}) \tag{1a}$$

$$\text{s.t. } s_{n,k} + s_{d,k+1} - 1 \leq 0 \tag{1b}$$

$$d - n + 1 \leq 0 \tag{1c}$$

$$\mathbf{S}^T \mathbb{1}_{N\times 1} - \mathbb{1}_{K\times 1} = \mathbb{O}_{K\times 1} \tag{1d}$$

where the following quantities have been introduced:

- $\mathbf{S} \in \{0,1\}^{N,K}$ is a binary matrix recording the matches. Each entry $s_{n,k}$, when set to one, describes a pairwise match between $\mathbf{P}_k$ and the n-th row of $\mathbf{P}_{\text{AID},k}$, denoted as $\mathbf{P}_{\text{AID},k}^{(n)}$. $\mathbf{S}^*$ is the result of the optimal match.
- $f(\mathbf{P}, \mathbf{P}_{\text{AID}}, \mathbf{S})$ is the global cost function used for matching the two VDMDSs depending on a specific $\mathbf{S}$-matrix. As a global cost function we consider the accumulated local cost, such that

$$f(\mathbf{P}, \mathbf{P}_{\text{AID}}, \mathbf{S}) = \sum_{n=1}^{N} \sum_{k=1}^{K} c\left(\mathbf{P}_k, \mathbf{P}_{\text{AID},k}^{(n)}\right) s_{n,k} \tag{2}$$

where c is the local cost function. Indeed, to compute the global cost, it may be effective to use a local cost and implement it through a Distance Function (DF), which measures the distance between two samples. L_p distances can be adopted as DFs.

It is possible to differentiate between L_p distances when referring to norms with $p \geq 1$ and *quasi-distance* functions when considering L_p quasi-norms $0 < p < 1$. The L_p DF characterized by $p = 0$ is associated to a pseudo-norm, but is a legitimate DF [11]–[14].

The solution to (1) is subject to specific constraints.

- *Monotonic match*. Given a match of $\mathbf{P}_k$ with $\mathbf{P}_{\text{AID},k}^{(n)}$, then $\mathbf{P}_{k+1}$ can be matched to the aiding samples going from n to N. Hence, the SM algorithm cannot go back in time (cf. (1b) and (1c)).
- *Match uniqueness*. Each $\mathbf{P}_k$ can only have one associated aiding sample (cf. (1d)).

B. Dynamic Time Warping

Different SM methods exist in the literature. However, in this work, Dynamic Time Warping (DTW) [15], [16] is chosen because of its flexibility and customizability. DTW is a classical SM technique that leverages dynamic programming [15] to allow one-to-many matches by stretching or compressing sequences. It solves an optimization problem similar to (1) through the construction of three matrices:

- Cost matrix $\mathbf{C} \in \mathbb{R}^{N,K}$: Stores the matching costs between samples of the two sequences, computed using a DF (see Section II-A).
- Accumulated cost matrix $\mathbf{G} \in \mathbb{R}^{N,K}$: Built recursively from $\mathbf{C}$, it contains the cumulative cost of matching sequence pairs up to a given index.
- Direction matrix $\mathbf{D} \in \mathbb{S}^{N,K}$, with $\mathbb{S} := \{1, 2, 3\}$: Defines the optimal matching path and is constructed alongside $\mathbf{G}$.

The optimal matching path is retrieved via backtracking, preventing local minima [16]. However, the standard DTW output does not comply with (1d), as multiple samples of $\mathbf{P}_{\text{AID},k}^{(n)}$ can be assigned to a single $\mathbf{P}_k$ sample. To ensure that each GNSS observable-based trajectory sample corresponds uniquely to an OBAT sample, a pruning step is applied to the matches obtained by DTW.

In particular, given $\mathbf{P}_k$ and a set of matched $\mathbf{P}_{\text{AID},k}^{(n)}$ it is then considered only the couple characterized by the lowest local cost $c(\mathbf{P}_k, \mathbf{P}_{\text{AID},k}^{(n)})$. The output of the algorithm is a VDMDS $\hat{\mathbf{P}}_{\text{AID}} = \{\hat{\mathbf{P}}_{\text{AID},1}, \ldots, \hat{\mathbf{P}}_{\text{AID},k}, \ldots, \hat{\mathbf{P}}_{\text{AID},K}\}$ composed by the samples that are exclusively matched to a specific sample of $\mathbf{P}_k$, where $\mathbf{P}_{\text{AID},k} \in \mathbb{R}^{1,2L_k}$.

The SM problem is also solved applying a local weighting technique on the $\mathbf{G}$ matrix which exploits the knowledge of the local costs enclosed in $\mathbf{C}$. This lead to a weighted accumulated cost matrix

$$\mathbf{W}_{\mathbf{G}} = \mathbf{C}^{\circ\gamma} \odot \mathbf{G} \; . \tag{3}$$

where $\gamma \in \mathbb{R}^+$ can be tuned to increase or decrease the weighting. This strategy was developed in a previous research [10] with the goal of improving the match accuracy.

III. Methodology

The proposed DTW customization is extensively tested and validated on realistic GNSS data from the LuGRE QN400-Space GNSS receiver [17]. These data were collected during the preparatory phase of the mission, in the context of scientific analyses conducted through a Hardware In the Loop (HIL) simulation testbed.

To extract GNSS observables (i.e., pseudorange and pseudorange rates), the receiver's front-end processed Radio Frequency (RF) signals generated by the Spirent GSS9000 simulator, which was controlled via the SimGEN software [18]. The simulated signals included Global Positioning System (GPS) (L1, L5) and Galileo (E1, E5) bands. To drive SimGEN and generate consistent signals it is used a pre-defined spacecraft trajectory $\mathbf{Y}$, referred to as the AT. This trajectory forms the basis of the OBAT, modified to provide the SM algorithm with challenging aiding data. Additionally, the dataset contains the sequence $\mathbf{P}$, which consists of GNSS observables computed by the receiver. Both trajectories are timestamped to Coordinated Universal Time (UTC) and sampled at 1 Hz.

A. OBAT synthetization

The main characteristic of this strategy is that the DTW performs a tight match directly on the measurements. However, before doing the match some pre-processing steps are needed. In particular, the OBAT $\mathbf{P}_{\text{AID}}$ it is obtained by a synthesis process involving

- the information on the satellite position enclosed in $\mathbf{X}_S = \{\mathbf{X}_{S1}, \ldots, \mathbf{X}_{Sk}, \ldots, \mathbf{X}_{SK}\}$, a VDMDS whose entries $\mathbf{X}_{Sk} \in \mathbb{R}^{L_k,6}$ contain the position and velocity in a three-dimensional space of L_k SVs for which measurements are available at epoch k.
- the AT that encapsulates a priori information on the spacecraft state, and may refer to a pre-designed trajectory that the spacecraft is intended to follow while traveling. It is associated to $\mathbf{Y} \in \mathbb{R}^{N,L}$ and each sample includes the spacecraft position and velocity states at the n-th epoch in a three-dimensional space (i.e. $L = 6$).
- the clock bias and drift for each epoch k. They can be obtained from a Precise Orbit Determination (POD) solution or derived using a clock-physics model.

At epoch k, each entry of $\mathbf{P}^{\rho}_{\text{AID},k}$ is synthesized as

$$\rho_{n,l_k} = \|\tilde{\boldsymbol{x}}_{l_k} - \tilde{\boldsymbol{y}}_n\|_2 + b_{ut,k-1} + \Delta t \dot{b}_{ut,k-1} \tag{4}$$

where:

- $\|\tilde{\boldsymbol{x}}_{l_k} - \tilde{\boldsymbol{y}}_n\|_2$ is obtained computing the Euclidean Distance (ED) between the l_k-th satellite and the n-th aiding sample. It is the LOS distance between the l_k-th satellite and the n-th aiding sample. In particular, $\tilde{\boldsymbol{x}}_{l_k}$ is a vector extracted from $\mathbf{X}_{\boldsymbol{S}k}$ containing only the position $[x_{S,l_k}, y_{S,l_k}, z_{S,l_k}]$ of a specific l_k-th satellite at a given epoch k. On the other hand, $\tilde{\boldsymbol{y}}_n$ is a vector extracted from $\mathbf{Y}$ containing only the position states of the AT $[x_n, y_n, z_n]$;
- $b_{ut,k-1}$ is the GNSS receiver clock bias at epoch $k-1$;

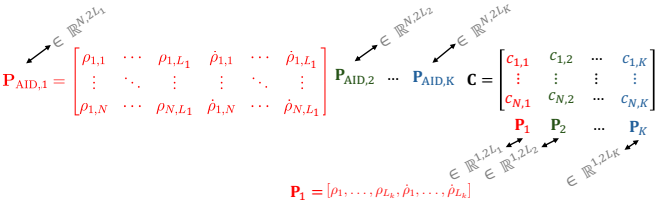

Fig. 1: Example of how $\mathbf{P}_{\text{AID}}$ and $\mathbf{P}$ contribute to the construction of the cost matrix $\mathbf{C}$ in the measurement domain.

- $\Delta t \dot{b}_{ut,k-1}$ is the linear propagation of the clock bias through clock drift at epoch $k-1$. In particular, Δt is the time interval between the two epochs.

At epoch k, each entry of $\mathbf{P}^{\dot{\rho}}_{\text{AID},k}$ takes the form

$$\dot{\rho}_{n,l_k} = (\dot{\tilde{\boldsymbol{x}}}_{l_k} - \dot{\tilde{\boldsymbol{y}}}_n) \cdot \frac{\tilde{\boldsymbol{x}}_{l_k} - \tilde{\boldsymbol{y}}_n}{\|\tilde{\boldsymbol{x}}_{l_k} - \tilde{\boldsymbol{y}}_n\|_2} + \dot{b}_{ut} \tag{5}$$

where:

- $\dot{\tilde{\boldsymbol{x}}}_{l_k} - \dot{\tilde{\boldsymbol{y}}}_n$ is the relative velocity between the l_k-th satellite and the n-th aiding sample. In particular, $\dot{\tilde{\boldsymbol{x}}}_{l_k}$ is a vector extracted from $\mathbf{X}_{\boldsymbol{S}k}$ containing only the velocities $[\dot{x}_{S,l_k}, \dot{y}_{S,l_k}, \dot{z}_{S,l_k}]$ of a specific l_k-th satellite at a given epoch k. On the other hand, $\dot{\tilde{\boldsymbol{y}}}_n$ is a vector extracted from $\mathbf{Y}$ containing only the velocity states of the AT $[\dot{x}_n, \dot{y}_n, \dot{z}_n]$;
- $\frac{\tilde{\boldsymbol{x}}_{l_k} - \tilde{\boldsymbol{y}}_n}{\|\tilde{\boldsymbol{x}}_{l_k} - \tilde{\boldsymbol{y}}_n\|_2}$ is the steering vector between the l_k-th and the n-th aiding;
- $\dot{b}_{ut}$ is the GNSS receiver clock drift, which is common for all the epochs k;

The main complication of this strategy is the presence of the variable dimension due to the variable number of SV in LOS. For this reason, during the DTW implementation, it must be considered that the distances associated with $\mathbf{P}_k$ are computed assuming the aiding $\mathbf{P}_{\text{AID},k}$ associated with the same epoch. Hence, the DTW is not based on one single aiding sequence but on K sequences, which are $\mathbf{P}_{\text{AID},k}$.
In particular, the critical step in the DTW implementation resides in the cost matrix. In Fig 1 is shown how matrix $\mathbf{C}$ it is built: for each column (hence for each $\mathbf{P}_k$) the costs are computed with respect to a different $\mathbf{P}_{\text{AID},k}$.

B. Validation, Data Adjustment, and Metrics

The validation of the DTW algorithm is performed by comparing the results with an exhaustive search applied to solve (1). However, it is not possible to apply the exhaustive search on the entire trajectory because it would result in an unfeasible computational time. In particular, only in the validation, this study applies the exhaustive search only to $K = 4$ epochs and $N = 30$ aiding samples. This kind of benchmarking is necessary to access the comparison between the DTW and an optimal technique. A complete analysis is carried out exploring different DFs. This approach made it possible to determine which DF is most suitable for a specific scenario.

To enhance the generality of the tested scenarios and challenge the SM algorithm, modifications were applied to the AT:

- Resampling at $f_s = 2\,\text{Hz}$ to analyze algorithm performance with different sample granularities, using Akima interpolation to reconstruct intermediate points.
- Temporal misalignment between GNSS measurement epochs and OBAT, simulated by adding a normally distributed error $\varepsilon \sim \mathcal{N}(0, \sigma^2_{\text{time}})$ to the resampled AT timestamps t_k.

The misalignment introduces a variable sampling rate, with a maximum non-overlapping $4\sigma_{\text{time}}$ determined iteratively using a finite search step to ensure conservativeness. This guarantees temporal consistency, preventing violations of $t_k + \varepsilon_k > t_{k+1} + \varepsilon_{k+1}$ with a 99.9937% probability.

To analyze the performances of the DTW is considered a dataset simulated at 60 RE located on the Low Lunar Orbit (LLO). The reason of considering a LLO scenario is to test the algorithm in a challenging RF visibility conditions.

The dataset is analyzed by examining the impact of time misalignment on OBAT, considering both a 'noisy timestamp' scenario ($\sigma_{\text{time}} = 0.06$ s) and a 'noiseless timestamp' case ($\sigma_{\text{time}} = 0$ s). In both cases, the DTW algorithm is evaluated in two configurations: non-weighted DTW (NW) and locally-weighted DTW (W) with $\gamma = 1$. All tests are performed using the customized DTW applied to (1), assessing the performance of different L_p DFs with p ranging from 0.01 to 30.

The study analysis is based on two metrics:

- **Accumulated Time Difference (ATD)**: This is a parameter allowing the evaluation of the time consistency in the alignment of the two VDMDS. The fundamental assumption for accessing the ATD is that both sequences are sharing the same time scale. This metric is analyzed for different L_p DF, while varying p.
- **Mismatch**: It represents the number of different matches given by the DTW and the exhaustive search depending on the value of p.

IV. Results and Discussion

Examining the ATD in the validation case, it is evident that both strategies (Locally-weighted and non-weighted DTW) behave similarly to the exhaustive search optimal approach. This observation becomes even more appreciable when considering the mismatch analysis. In particular, from Fig. 2 it can be observed that the number of mismatched samples is zero for all the tested DFs. This indicates that, for every L_p distance function analyzed, there is no difference in the matched samples between the exhaustive search and the DTW strategies. However, it is important to note that this result holds only for the analyzed window. When the validation is performed on a different window, the results can change.

For instance, analysis on a different window revealed that the classical strategy does not always align with the results of the exhaustive search, particularly for certain values of p where mismatches were observed. In both scenarios, the non-weighted DTW struggled to match the optimal approach for these p values. However, when $p \geq 0.6$, the ATD consistently converged to lower values.

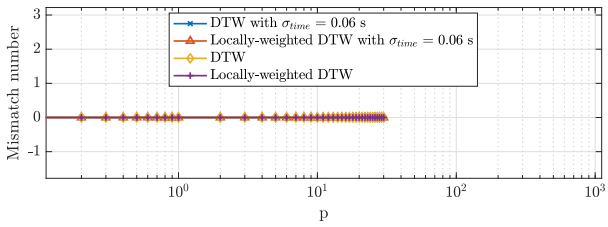

Fig. 2: Validation: DTW sample mismatch with respect to the exhaustive search at 60 RE.

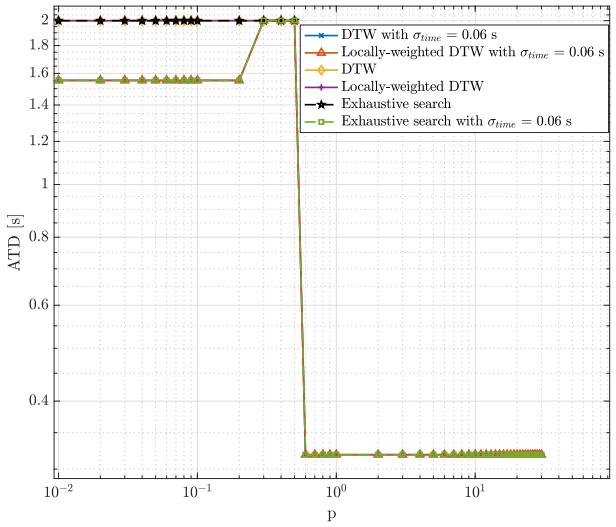

Fig. 3: Validation: ATD behavior as a function of p at 60 RE.

Extending the analysis to the entire window, it becomes apparent that the locally-weighted technique performs worse compared to the non-weighted strategy (see Fig. 4). The local weighting appears to stabilize a suboptimal solution in terms of ATD. The classical strategy yields better results initially exhibiting high ATD values, followed by a drop and eventual convergence to a steady level. The best outcome is observed at $p = 0.8$, where both non-weighted DTW strategies achieve their lowest respective values. This finding is further confirmed by the mismatch value (see Fig. 3).

V. Conclusion

After extensive validation and testing, the local weighting strategy showed no significant advantage in reducing ATD compared to the classical strategy. The best results were obtained with the classical approach, giving low ATD values, particularly for $p = 0.8$, indicating improved time consistency in the match. However, the chosen validation method is not entirely satisfactory. Evaluating the exhaustive search on a 4-sample window does not yield conclusive results, as the outcomes may not fully represent the entire trajectory. Indeed,

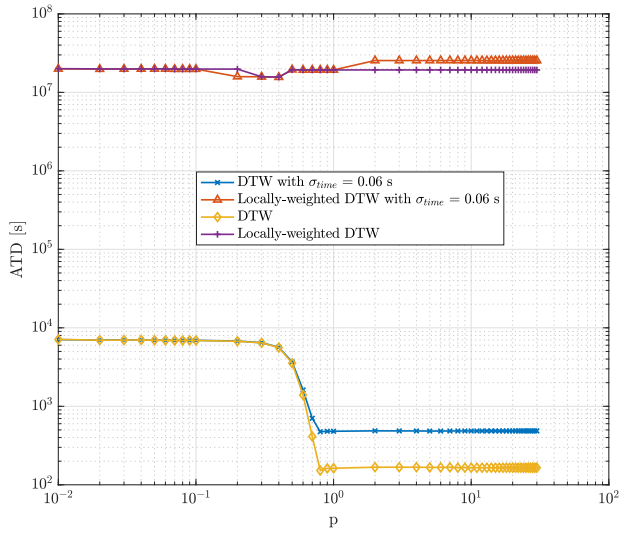

Fig. 4: ATD behavior as a function of p at 60 RE.

it can produce varying results across different windows. Nevertheless, the analysis still offers valuable insights into the optimality or sub-optimality of DTW.

Note that the selected p should be validated within a state estimation framework, as ATD is just an indicator of the best performing method and p, whose ultimate impact on state estimation can be assessed only through fusion filters optimally integrating the matched sequences.

The key advantage of applying SM in the observables domain is that it can be applied even with a single SV in LOS. However, since the number of LOS SVs varies, a new synthesized aiding must be generated at each epoch, increasing computational complexity. Future steps are the integration of these findings into an estimation framework, such as the TA-EKF, to evaluate and quantify the actual contribution of the SM method in a GNSS application. Moreover, extending the analysis to a less challenging scenario, such as at 17 RE, will provide further insights into the behavior of the algorithms.

Acknowledgment

This study was funded within the contract n. 2021-26-HH.0 ASI/Politecnico di Torino "Attività di R&S inerente alla Navigazione GNSS nello Space volume Terra/Luna nell'ambito del Lunar GNSS Receiver Experiment". The authors would like to thank Qascom and NASA for supplying the representative datasets of LuGRE operations that supported this study.

References

[1] NASA, "What is the Deep Space Network?" 2024. [Online]. Available: https://www.nasa.gov/directorates/somd/space-communications-navigation-program/what-is-the-deep-space-network/#hds-sidebar-nav-4

[2] H. H. Means, "The Deep Space Network: Overburdened and underfunded," *Physics Today*, vol. 76, no. 12, pp. 22–23, 2023.

[3] O. Vouch, A. Nardin, A. Minetto, S. Zocca, F. Dovis, L. Konitzer, J. Joel Parker, B. Ashman, F. Bernardi, S. Tedesco, and S. Fantinato, "Bayesian Integration for Deep-Space Navigation with GNSS Signals," in *2024 27th International Conference on Information Fusion (FUSION)*, 2024, pp. 1–8.

[4] O. Vouch, A. Nardin, A. Minetto, S. Zocca, M. Valvano, and F. Dovis, "Aided Kalman Filter Models for GNSS-Based Space Navigation," *IEEE Journal of Radio Frequency Identification*, vol. 8, pp. 535–546, 2024.

[5] J. J. K. Parker, F. Dovis, B. Anderson, L. Ansalone, B. Ashman, F. H. Bauer, G. D'Amore, C. Facchinetti, S. Fantinato, G. Impresario, S. A. McKim, E. Miotti, J. J. Miller, M. Musmeci, O. Pozzobon, L. Schlenker, A. Tuozzi, and L. Valencia, "The Lunar GNSS Receiver Experiment (LuGRE)," in *Proceedings of the ION ITM 2022 Conference*, NASA and Italian Space Agency (ASI). Long Beach, California: Institute of Navigation, 2022. [Online]. Available: https://ntrs.nasa.gov/api/citations/20220002074/downloads/LuGRE_ION-ITM_2022_Draft8_Submitted_ConferenceProceedings.pdf

[6] K. Schauer. (2023, 3) NASA Delivers Hardware for Commercial Lunar Payload Mission. NASA. Accessed: 2024-09-21. [Online]. Available: https://www.nasa.gov/missions/artemis/clps/nasa-delivers-hardware-for-commercial-lunar-payload-mission/

[7] L. Konitzer, J. J. Parker, B. Ashman, N. Esantsi, C. Facchinetti, F. Dovis, A. Minetto, A. Nardin, F. Bauer, L. Ansalone, and et al., "Science Objectives and Investigations for the Lunar GNSS Receiver Experiment (LuGRE)," in *Proceedings of the 37th International Technical Meeting of the Satellite Division of The Institute of Navigation (ION GNSS+ 2024)*, Sep 2024. [Online]. Available: https://doi.org/10.33012/2024.19711

[8] V. Capuano, F. Basile, C. Botteron, and P.-A. Farine, "GNSS-based Orbital Filter for Earth Moon Transfer Orbits," *The Journal of Navigation*, vol. 69, no. 4, pp. 745–764, 2016. [Online]. Available: https://doi.org/10.1017/S0373463315000843

[9] V. Capuano, E. Shehaj, C. Botteron, P. Blunt, and P.-A. Farine, "An Adaptive GNSS-based Reduced Dynamic Approach for Real Time Autonomous Navigation from the Earth to the Moon," in *Proceedings of the Pacific PNT 2017 Conference*. Honolulu, Hawaii: ION, 5 2017.

[10] F. Fiorina, O. Vouch, A. Nardin, F. Dovis, C. Facchinetti, and M. Musmeci, "A sequence matching approach for gnss-based orbit determination using dynamic time warping," in *2025 IEEE/ION Position, Location and Navigation Symposium (PLANS)*, 2025, pp. 1055–1065.

[11] W. Rudin, *Functional Analysis*, 2nd ed. New York: McGraw-Hill, 1991.

[12] C. C. Aggarwal, A. Hinneburg, and D. A. Keim, "On the Surprising Behavior of Distance Metrics in High Dimensional Space," in *Proceedings of the 8th International Conference on Database Theory (ICDT 2001)*, ser. Lecture Notes in Computer Science, vol. 1973. Berlin, Heidelberg: Springer-Verlag, 2001, pp. 420–434. [Online]. Available: https://doi.org/10.1007/3-540-44503-X_27

[13] S. Boyd and L. Vandenberghe, *Convex Optimization*. Cambridge, UK: Cambridge University Press, 2004, section A.1.3 - Examples of norms, including Euclidean and Manhattan distances.

[14] A. Le Franc, J.-P. Chancelier, and M. De Lara, "The Capra-subdifferential of the l0 pseudonorm," 2021, preprint submitted on 30 Dec 2021 (v1), last revised 25 Jan 2023 (v3).

[15] H. Sakoe and S. Chiba, "Dynamic Programming Algorithm Optimization for Spoken Word Recognition," *IEEE Transactions on Acoustics, Speech, and Signal Processing*, vol. 26, no. 1, pp. 43–49, 1978.

[16] M. Müller, *Information Retrieval for Music and Motion*. Berlin, Heidelberg: Springer-Verlag Berlin Heidelberg, 2007, with 136 Figures, 41 in color and 26 Tables.

[17] F. Dovis, A. Nardin, A. Minetto, C. Facchinetti, M. Musmeci, G. Varacalli, J. J. K. Parker, L. Konitzer, S. Sanathanamurthy, L. Valencia, J. J. Miller, F. H. Bauer, S. Fantinato, E. Miotti, M. Boschiero, M. Pulliero, S. Tedesco, F. Bernardi, and S. Guzzi, "Assessing the Usability of GNSS on The Way To The Moon: Getting The LUGRE Payload Ready To Fly," in *Proceedings of the 74th International Astronautical Congress (IAC)*. Baku, Azerbaijan: International Astronautical Federation (IAF), 10 2023.

[18] Spirent, "GSS9000 GNSS Simulator," Spirent Communications, Crawley, UK, 2015.